

Ursula Eicker, Antoine Dalibard
Photovoltaic thermal collectors for night radiative cooling of buildings
Solar Energy (2011), Volume 85, Issue 7, pp 1322-1335

Photovoltaic thermal collectors for night radiative cooling of buildings

Ursula Eicker, Antoine Dalibard

Center of Applied Research Sustainable Energy Technologies zafh.net, University of Applied
Sciences Stuttgart, Germany, Schellingstraße 24, 70174 Stuttgart

Tel: +49 711 8926 2831, Fax: +49 711 8926 2698, Email: ursula.eicker@hft-stuttgart.de

ABSTRACT

A new photovoltaic-thermal (PVT) system has been developed to produce electricity and cooling energy. Experimental studies of uncovered PVT collectors were carried out in Stuttgart to validate a simulation model, which calculates the night radiative heat exchange with the sky. Larger PVT frameless modules with 2.8 m² surface area were then implemented in a residential zero energy building and tested under climatic conditions of Madrid. Measured cooling power levels were between 60 and 65 W m⁻², when the PVT collector was used to cool a warm storage tank and 40 to 45 W m⁻², when the energy was directly used to cool a ceiling. The ratio of cooling energy to electrical energy required for pumping water through the PVT collector at night was excellent with values between 17 and 30. The simulated summer cooling energy production per square meter of PVT collector in the Madrid/Spain climatic conditions is 51 kWh m⁻² a⁻¹. In addition to the thermal cooling gain, 205 kWh m⁻² a⁻¹ of AC electricity is produced under Spanish conditions. A comparative analysis for the hot humid climate of Shanghai gave comparable results with 55 kWh m⁻² a⁻¹ total cooling energy production, mainly usable for heat rejection of a compression chiller and a lower electricity production of 142 kWh m⁻² a⁻¹.

Keywords: PVT, radiative cooling, zero energy building

1. Introduction

Radiative cooling of buildings has attracted considerable research over the years, much of it focused on evaluating the magnitude of the resource and the variations in cooling potential for different locations (Erell and Etzion, 2000 [24], Dimoudi and Androutsopoulos, 2006 [20], Farahani et al, 2010 [26], Argiriou et al, 1994 [1]). However, radiative cooling is still not applied in today's buildings, as there are no commercially available components. A further barrier to more widespread use of radiative night cooling is the low power density, which requires large roof surface areas and rather high mounting costs. On the other hand, many buildings are now completely covered with photovoltaic panels for solar electricity production. A low cost combination of photovoltaic modules with a thermal collector (PVT) could provide a very interesting and cost effective solution for radiative cooling applications.

Radiative cooling is based on the heat loss by long-wave radiation emission towards the sky. Sky temperature during summer nights can be less than 0°C, under clear summer night sky conditions sky temperatures of -10°C are possible. This corresponds to relative temperature depressions between of 20-30K. The long wave radiation is mainly dependent on the water content of the atmosphere, with 90% of the sky radiation originating from the first kilometer above ground and 40% from only 10 m above ground (Bliss, 1961 [13]). Therefore the radiation strongly varies from site to site.

Different radiative cooling applications have been investigated, such as movable insulation, air based systems and open or closed water-based systems. The specific cooling power measured ranges from 20 to 80 W/m² (Cavelius, 2005 [16]). One of the first applications of radiative cooling tested about 50 years ago was the movable insulation. The roof insulation is removed during the night in order to cool down the building through radiation towards the

sky. The major drawback of such system is the motor-operated system to remove and replace the insulation panels (Santamouris, 2007 [35]). Others early experiments with radiative cooling were carried out in Israel at the beginning of the 70s. They were based on radiative cooling of air flowing in a narrow channel. A similar system combined with a solar chimney for winter was investigated by Brunold (1989) [15]. The maximum cooling output of the system under favourable environmental conditions was 17 W m^{-2} .

Since water has a higher heat capacity, water-based systems can be better controlled and operated with a low electrical energy input. One of the first applications of a radiative cooling water-based system was investigated by Juchau (1981) [30], who used a standard flat plate collector coupled with a storage tank to cool down water during the night. The cold water was used during the day to cool down the building through a concrete floor slab. This concept was further developed in Israel by Erell and Etzion (1992) [23]. By removing the cover, they obtained a net cooling power of 81 W m^{-2} for seven hours of operation each night over a three week period in the summer of 1990.

Open water-based systems have been investigated more recently in Germany (Beck, 2006 [5]). This approach consists of letting the water flow on a tilted surface. Due to the high emissivity of water (typically 0.96) and since there is no additional thermal resistance between the water and the ambient, the expected cooling outputs are higher than for closed systems. Measurement data of the demonstration plant installed in Würzburg (Germany) show that a specific cooling power of 120 W m^{-2} can be achieved. With the cooperation of the University of Applied Sciences Stuttgart (UAS), a similar system has been planned for the Solar Decathlon 2007 by the Technical University of Darmstadt, winner of the competition.

Within the European Solar Decathlon competition taking place in Madrid in June 2010, the Stuttgart University of Applied Sciences developed a completely renewable powered zero

energy building named Home+ with a useful floor area of 56 m². The building is equipped with a radiative cooling system using hybrid photovoltaic-thermal (PVT) collectors.

2. PVT collector design and applications

Although open systems can achieve higher cooling output, their integration into the cooling distribution system presents some drawbacks compared to closed systems. Since the water is in direct contact with the atmosphere, a filter is necessary to prevent dust to enter the system. The system works at atmospheric pressure and therefore has to be decoupled from the distribution system with a heat exchanger between the radiant cooling loop and the building cold distribution. Furthermore, the water consumption due to evaporation is not negligible. Simulation studies showed that a nightly consumption of about 0.1 kg m⁻² (3.5 kg/ night in total for the building) can be expected for the Madrid climate conditions if an open system is chosen. For those reasons a closed water-based system with PVT collectors has been chosen. Water based PVT collectors are normally used only during the day for electricity generation and thermal energy production. Depending on the application, the main objective is either the electricity production or the thermal output. In the first case, the fluid has to cool down the PV cells as much as possible increase their efficiency. In the second case, one expects a certain outlet temperature of the fluid for a given application (domestic hot water, thermal cooling etc.). The design of the PVT collector will depend mainly on the objective defined. Figure 1 shows the two main types of PVT collectors available on the market which are uncovered and covered.

The International energy agency lists about 50 projects with PVT collectors in the last 25 years with less than 20 of them using water (Hansen, 2007 [28]). Most projects were done in Europe, especially the Netherlands and Great Britain. Furthermore there are some projects in Thailand using large amorphous silicon modules in a PVT collector, where electricity and

warm water is produced for hospitals and public buildings (Jaikla et al, 2005 [29]). For the thermal collector both metallic and polymer materials are used (Meir et al, 2002 [33], Cristofari et al, 2009 [19]). Both water and air are used as heating fluid (Tripanagnostopoulos, 2007 [37]). Apart from direct heating applications, PVT collectors have also been used as evaporators in compression heat pump systems (Chen et al, 2010 [17], Fang et al, 2010 [25], Bertram et al, 2010 [10]).

To the knowledge of the authors, PVT collectors have not yet been used for night radiative cooling applications. This kind of application requires a special construction of the PVT module which allows a maximum heat loss by long-wave radiation emission from the PVT collector toward the sky. That is why the uncovered design has been chosen. Furthermore, the thermal contact between the absorber and the PV module has to be as good as possible. For the cooling application described in this work, a covered commercial PVT collector from the PVTwins company has been used, where the cover was removed. The uncovered PVT collectors have been tested on the roof of Stuttgart UAS to evaluate the cooling potential during the night. However, as the collectors were not available in the dimensions required for the Solar Decathlon building, an own collector construction was chosen.

3. The zero energy building Home+ and its energy supply system

The Stuttgart Solar Decathlon building named Home+ is a highly insulated passive standard building with U-values of the facade and roof construction between 0.1 and 0.16 W m⁻² K⁻¹. Triple glazed windows with U-values of 0.52 W m⁻² K⁻¹ and g-values of 0.58 provide excellent thermal properties with very low heat losses or gains.

Thermal mass is provided by phase change materials (PCM) with a total surface area of 18 m² (1 cm thick, density of around 1500 kg m⁻³). With a melting temperature of about 22°C, the latent heat of the PCM is used for both cooling and heating purposes and smoothes the temperature variation in the room. In summer, the PCM ceiling is actively regenerated by a

water based distribution system, which uses only cooling energy provided by the PVT collectors.

Heat and cold is also distributed by a radiant floor (30 m²), which is connected to a reversible heat pump with 2.4 kW cooling power. The radiant floor can also be operated in free cooling mode in summer. In this case, cold water is taken directly out of the heat sink tank and pumped to the radiant floor. This free cooling mode is only possible when the temperature in the tank is below 19°C. The tank can only be cooled down by radiative cooling of the PVT modules.

The PV system with a peak power of 12.5 kW consists of 66 m² of polycrystalline surface on both east/west facades and part of the roof and 33 m² of monocrystalline cells for the PVT modules (see Figure 2). A further 5 m² of the roof area are covered with PVT modules, which do not produce electricity, but only cooling, as they are mostly shaded by the ventilation tower.

The PVT module are frameless glas/glas modules with 1.194 m x 2.324 m dimensions and an electrical power of 410 W_p per module. The electric efficiency is 14.7%. The PVT modules are mounted horizontally on the roof (see Figure 3).

The main priority of the PVT collectors is to regenerate the PCM ceiling and then to cool down the 1.2 m³ storage tank used as a heat sink for the compression chiller during the day. Only if the storage tank temperature is too high (above 45°C), the heat store is cooled down first. If the storage tank temperature is low enough at 19°C, the water can be used directly for free cooling operation of the radiant floor.

Figure 4 shows the system technology for heating and cooling including the PVT collectors.

The PVT collectors are made of copper tubes with 15 mm internal and 17 mm external diameter held within aluminium strips. The aluminium is glued to the PV module with an epoxy resin glue with improved thermal conductivity (see Figure 5).

The volume flow through the PVT collectors is $20 \text{ kg m}^{-2} \text{ h}^{-1}$, provided by an electrical pump of 85 W power.

4. Thermal modelling of the PVT collector

4.1. Modelling approach

Modelling of flat plate thermal collectors has been extensively detailed in the literature (Duffie and Beckmann, 2006 [21]). This model has been adapted for an uncovered flat plate collector used for radiative cooling application (Erell and Etzion, 2000 [24]).

Based on this approach, first the overall heat loss coefficient of the collector (from the absorber to the ambient) has to be calculated. For an uncovered and non-insulated PVT collector, the thermal circuit diagram is shown in Figure 6.

The overall heat transfer coefficient (U-value) is obtained from the sum of the two parallel conductances:

$$U_t = \frac{1}{R_f} + \frac{1}{R_b} \quad (1)$$

The front resistance R_f includes the conductive resistance of absorber and PV module R_3 , the convective resistance to ambient air R_2 and the resistance due to radiative exchange with the sky R_1 .

$$R_f = \frac{R_1 R_2}{R_1 + R_2} + R_3 \quad (2)$$

The resistance of the back surface R_b is calculated from the parallel radiative and convective resistances R_4 and R_5 :

$$R_b = \frac{R_4 R_5}{R_4 + R_5} \quad (3)$$

4.2. Calculation of thermal resistance R_1

In order to integrate the net radiative heat losses into the overall U-value of the collector model, the heat transfer coefficient is normalized by the temperature difference between PV cover and ambient air.

$$h_r = \sigma \epsilon_{PV} \frac{(T_{PV}^4 - T_{sky}^4)}{T_{PV} - T_{amb}} \quad (4)$$

with $R_1 = \frac{1}{h_r}$

4.3. Calculation of thermal resistance R_2

The thermal resistance R_2 due to mixed convection between the PV cover and the environment is expressed as followed:

$$R_2 = \frac{1}{h_{c,mix}}$$

The heat transfer coefficient for mixed convection is expressed as a function of the heat transfer coefficients for forced and free convection:

$$h_{c,mix} = \sqrt[3.5]{h_{c,forced}^{3.5} + h_{c,free}^{3.5}}$$

The heat transfer coefficients for forced and free convection have been calculated using the correlations given in [ASHRAE, [2]) for external flows on horizontal plates.

4.4. Calculation of thermal resistance R_3

The calculation of the thermal resistance of the PV module requires construction details of a PV module. A typical configuration of laminated and encapsulated silicon solar cells with 3 mm glass and 0.1 mm Tedlar back surface was used for the PVTwins prototype testing.

The thermal resistance of the PV module plus glue (resistance R_3) for a glue thickness of 0.1 mm and a thermal conductivity of 0.85 W/(mK) gives a resistance $R_3 = 0.0079 \text{ m}^2 \text{ K W}^{-1}$. The glue used is a mixed of epoxy resin and aluminium in order to enhance thermal conductivity. The larger PVT modules used in the Home⁺ building have a higher glass thickness of 1.4 cm for structural reasons. Also the glue thickness is higher with 1 mm, resulting in a total thermal resistance $R_2 = 0.02 \text{ m}^2 \text{ K W}^{-1}$.

4.5. Calculation of thermal resistance R_4 and R_5

The radiative thermal resistance between the horizontal absorber plate and the horizontal roof R_4 is calculated for two parallel plates, the thermal resistance R_5 is due to natural convection between the absorber and the ambient and is calculated according to (ASHRAE, [2]) for external flows on horizontal plates.

4.6. Fin efficiency, collector efficiency and collector removal factor

Next the overall heat transfer coefficient U can be determined. As the convective and especially the radiative heat transfer coefficients are temperature dependent, an iteration process has to be used.

The collector efficiency factor F' is calculated using the fin efficiency of the copper absorber and the tubes as for a standard flat plate collector. The conduction within the glass module with its low conductivity is negligible compared to the 0.2 mm aluminium absorber with a thermal conductivity of $220 \text{ W m}^{-1} \text{ K}^{-1}$. With the collector efficiency factor F' and the mass flow through the thermal collector the heat removal factor F_r can be calculated.

The difference with the Duffie and Beckmann approach for standard thermal collectors is that the short wave irradiation is in this case zero.

$$\dot{Q}_u = AF_R \left(U_t (T_{f,in} - T_{amb}) \right) \quad (5)$$

4.7. Model limitations

Condensation has not been taken into account in the model which is one of the approximations/limitations of the model. However previous work shows that condensation gains should not be overestimated for uncovered thermal collectors especially in the summer period. Bertram et al. investigated the heat gain condensation of a ground coupled heat pump with uncovered collectors, and he shows that the performance of the system is only marginally improved by 3.8% over the all year. The improvement is much higher in winter (13%) than in summer (less than 1%) (Bertram, 2010, [11]). Furthermore, in order to take into account this limitation in the model, for the yearly simulation, the night radiative cooling system with PVT collectors were not operated when the inlet water temperature was below the dew point temperature of the ambient air. This limits the error committed when neglecting the condensation heat gains.

5. Modelling of sky temperatures

A good estimation of the sky temperature is crucial when modelling the performance of radiative cooling systems. The concepts of effective sky temperature T_{sky} , and effective sky emissivity ε_{sky} have been introduced to determine the infrared sky radiation. The actual net radiation heat exchange $Q_{sky,net}$ between a body of surface A with emissivity ε at T_{sky} is given by:

$$\dot{Q}_{sky,net} = \varepsilon\sigma A(T_{body}^4 - T_{sky}^4) \quad (6)$$

where σ is the Stefan-Boltzmann constant.

The sky can be considered as a blackbody ($\varepsilon=1$) at the effective sky temperature. The effective sky temperature is defined as:

$$T_{sky} = \left(\frac{\dot{Q}_{sky}}{\sigma} \right)^{\frac{1}{4}} \quad (7)$$

where \dot{Q}_{sky} is the incoming atmospheric thermal irradiance. In order to relate the sky temperature and the ambient temperature (dry bulb), the concept of effective sky emissivity is defined as a grey emitter with the same temperature as the ambient temperature:

$$T_{sky} = \varepsilon_{sky}^{\frac{1}{4}} T_{amb} \quad (8)$$

Combining the last two equations gives:

$$\varepsilon_{sky} = \frac{\dot{Q}_{sky}}{\sigma T_{amb}^4} \quad (9)$$

Many models based on empirical or semi-empirical correlations are available in the literature to calculate the effective emissivity (respectively sky temperatures). Most of them are valid only for clear sky conditions, others apply some factors to take into account the cloudy conditions.

Clear sky models

The simplest models use the dry bulb temperature alone to estimate T_{sky} (Swinbank (1963) [36], Fuentes (1987) [27]). More advanced models take into account the influence of the humidity by using either the partial pressure of water vapour or the dew point temperature.

Berdahl and Martin (1984) [7] introduced additional correction factors to their correlation to account for the differences in radiative transfer between the night time black sky and the day time blue sky and for the elevation of the observing station. Table 2 shows a non exhaustive list of some models available to calculate effective sky emissivity or temperatures for clear sky conditions:

According to long term measurements at 11 different stations in USA, these simple models for clear sky (especially those which only use the dry bulb temperature) can produce huge errors (Atwater and Ball, 1978, [3]). This is mainly due to the fact that the cloudiness is not taken into account.

Cloudy sky models

For totally cloudy skies, the international norm ISO 6946 suggests to take the sky temperature equal to the ambient temperature. Nevertheless, better estimations are needed for intermediate conditions.

To account for the cloudiness and correct the existing clear sky models, different factors have been used. Kasten et al. (1980) [31] used a cloudiness factor C_{cover} (between 0 and 1) to characterize the fraction of sky, which is covered by clouds. C_{cover} is determined by measurements of global irradiation G and diffuse fraction of global irradiation G_d :

$$C_{\text{cover}} = \left(1.4286 \frac{G_d}{G} - 0.3 \right)^{0.5} \quad (10)$$

The sky emissivity for a cloudy sky is then calculated as followed:

$$\varepsilon_{sky} = \varepsilon_{sky,clear} + 0.8(1 - \varepsilon_{sky,clear})C_{cover} \quad (11)$$

Aubinet (1994) [4] introduced a sky clearness index K_0 , which is the ratio between global solar horizontal radiation G_h to the extraterrestrial solar irradiation G_0 :

$$K_0 = \frac{G_h}{G_0} \quad (12)$$

The sky temperature is then calculated as followed:

$$T_{sky} = 94 + 12.6 \ln p_d - 13K_0 + 0.341T_{amb} \quad (13)$$

Another approach to account for the cloudiness has been developed by Perraudau (1986) [34]. The Perraudau's nebulosity index is defined as:

$$l_p = \frac{1 - \frac{D_h}{G_h}}{1 - \frac{D_c}{G_c}} \quad (14)$$

D_h is the diffuse irradiance on a horizontal plane [W/m²]

G_h is the total irradiance on a horizontal plane [W/m²]

D_c is Bird model total diffuse solar irradiance on horizontal surface for clear sky [W/m²]

G_c is Bird model direct solar irradiance on horizontal surface for clear sky [W/m²]

Bird's model is a diffuse model widely used to calculate the hourly clear sky irradiation on a defined horizontal surface (1981) [12]. The nebulosity index is then used to determine a cloud cover factor which uses another scale (N=0 for cloudless skies and N=8 for overcast skies):

$$\begin{aligned}
 N &= 8 && \text{if } l_p \leq 0.07 \\
 N &= INT \left(\sqrt[8]{\frac{1-l_p}{0.825} + 0.5} \right) && \text{if } 0.07 < l_p < 1 \\
 N &= 0 && \text{if } l_p \geq 1
 \end{aligned} \tag{15}$$

For annual simulation of PVT performance, the simulation software TRNSYS was used. The sky models are based on the corrected correlation of Berdahl and Martin [8] to calculate the clear sky emissivity. Type 15 uses the following formula:

$$\varepsilon_{sky} = \varepsilon_{sky,clear} + (1 - \varepsilon_{sky,clear}) f_{cloud} \varepsilon_{cloud} \tag{16}$$

where f_{cloud} is the fraction of the sky that is covered by clouds (between 0 and 1) and ε_{cloud} is the emissivity of the clouds themselves (here constant with 0.9). Those values are read from the weather files. To generate the weather data, the software Meteonorm was used with the approach of Perraudau to estimate N and calculate the cloud cover fraction f_{cloud} .

The main problem with existing cloudy sky models is that they are based on daytime clearness indices and result in one constant value for the night. Thus the time series of sky temperatures cannot be adequately represented, as moving clouds cannot be considered.

6. Experimental set-up for the prototype testing and the home+ measurements

Two PVTwin modules from the company PVTwins/ZenRenewables were used to validate the theoretical model. They are available on the market since 2008 with dimensions of 2.8 up to 4.2 m² and an electrical efficiency of 13%. The modules are normally used for combined electricity and heat production, i.e. the combined PV-absorber element is covered by a glass sheet to reduce heat losses. For the experiments, the cover glass was removed to allow long wave radiative exchange with the sky and the modules were not electrically connected. One of the PVT modules was completely uninsulated, the other had a backside insulation. The dimensions of the prototypes are 0.80 m x 0.827 m. The absorber tube length is 5.92 m with an internal diameter of 8 mm and an external diameter of 10 mm. The total water content is thus 297 ml. Figure 7 shows the dimensions of the collector tested. The emissivity of the uncovered PVTwin collector was measured as 0.8978.

A 270 liters tank with a 3 kW electrical heater is used to store the cold water and heat the water during the day. The surface temperature of the PV module is measured by two thermocouples, one positioned at the fluid inlet and the other at the outlet (± 0.1 K accuracy). The inlet and outlet fluid temperatures are measured in the fluid with PT100 sensors (± 0.1 K accuracy), the mass flows with magnetic inductive flow meters (Krohne IFC 090 K, accuracy $\pm 0.5\%$). The sky temperature was measured using a pyrgeometer (Kipp and Zonen CGR3, 5% measurement accuracy). In addition, wind velocity (± 0.3 m/s accuracy), wind direction ($\pm 1.5^\circ$ accuracy), daytime global and diffuse radiation ($\pm 2\%$ accuracy), ambient temperature (± 0.3 K accuracy) and relative humidity ($\pm 0.2\%$ accuracy) were measured. The data acquisition of all the measured values has been done with a datalogger Agilent HP 34970A. The experimental results were used to validate the model described before. The results discussed are for the uninsulated collector only, as the goal is maximum heat losses during night. All measurements were carried out in autumn 2009.

The measurements of the PVT collectors integrated in the home+ building were carried out in June 2010. A weather station was installed for temperature (± 0.1 K accuracy), humidity ($\pm 0.2\%$ accuracy), irradiance ($\pm 2\%$ accuracy), wind direction ($\pm 5^\circ$ accuracy) and wind velocity ($\pm 3\%$ accuracy). Surface temperature sensors were used for inlet/outlet water temperatures and also at the back of the PVT absorber. Three immersed PT100 temperature sensors (± 0.1 K calibration accuracy) were used to measure the temperature stratification within the heat sink tank and to determine the change of energy content. As the installed energy meters measuring PVT energy production were not properly functioning during the competition week, the energy delivered by the PVT collectors to the heat sink tank was obtained from the average temperature changes measured in tank. The error for the energy content change was determined by using a lower accuracy of temperature measurements of only ± 1 K, as the equidistant positioning cannot be accurately determined.

The flow rate through the PVT collectors when connected to the PCM ceiling, was measured during the building commissioning and was $10 \text{ kg m}^{-2} \text{ h}^{-1}$. The data acquisition has been done using a building automation system from Beckhoff.

7. Results from prototype measurements

Temperature levels of the PVT collector were measured together with ambient air and sky temperatures to determine the achievable power levels as a function of temperature difference. The mean mass flow rates were $23 \pm 0.115 \text{ kg m}^{-2} \text{ h}^{-1}$ during the first night and $28 \pm 0.14 \text{ kg m}^{-2} \text{ h}^{-1}$ during the second night. The deviations in the measured and simulated return water temperature are less than 0.5 K during the night (see Figure 8). During the day, obviously the shortwave irradiance dominates and the model does not work well.

The cooling power \dot{Q}_c was calculated from the measured temperature difference between inlet and outlet (T_{in} and T_{out}), the mass flow rate \dot{m} and the water heat capacity c_p .

$$\dot{Q}_c = \dot{m}c_p (T_{in} - T_{out}) \quad (17)$$

The resulting cooling power at night varies between 100 and 120 W m⁻² (see Figure 9). The uncertainty in the measured cooling power was calculated using Gaussian errorpropagation.

$$\begin{aligned} \sigma_{\dot{Q}_c} &= \sqrt{\left(\frac{\partial \dot{Q}_c}{\partial \dot{m}}\right)^2 \sigma_{\dot{m}}^2 + \left(\frac{\partial \dot{Q}_c}{\partial T_{in}}\right)^2 \sigma_{T_{in}}^2 + \left(\frac{\partial \dot{Q}_c}{\partial T_{out}}\right)^2 \sigma_{T_{out}}^2} \\ &= \sqrt{\left(c_p (\bar{T}_{in} - \bar{T}_{out})\right)^2 \sigma_{\dot{m}}^2 + (\bar{\dot{m}}c_p)^2 \sigma_{T_{in}}^2 + (\bar{\dot{m}}c_p)^2 \sigma_{T_{out}}^2} \end{aligned} \quad (18)$$

For the first night from 18.-19.11. the mean cooling power was 119.7 ± 6.3 W m⁻², for the second night 107.0 ± 7.2 W m⁻².

Further measurements were done using higher water inlet temperatures to study the effect of temperature difference between fluid and sky (see

Figure 10).

The maximum deviation in outlet temperature between simulated and measured values is less than 2K. The deviation in the global energy balance over the period is less than 1 %.

If the cooling power is plotted versus the temperature difference between fluid inlet and calculated sky temperature, the range of achievable cooling power can be seen. At temperature differences of $30 \pm 1 \text{ K}$ between PVT collector and sky, the mean specific cooling power is $120.3 \pm 6.3 \text{ W m}^{-2}$ (see Figure 11).

Finally different sky temperature models were compared with the measured sky temperature from the pyrgeometer. The measurements were carried out during clear sky nights and cloudy nights. Good agreement was generally given by the correlations of Berdahl/Martin and Chen during clear sky conditions, all other correlations resulted in higher temperature levels than measured except of Elsasser correlation. If the sky is cloud covered, the measured temperature levels rise strongly and the clear sky models fail (see Figure 12). Also cloudy sky correlations of the literature have been compared to the measured sky temperature. As expected, large deviations are observed during clear sky conditions, whereas during cloudy conditions the accuracy of the correlation depend strongly on the cloudy factor (or clearness index) that have been calculated with the ration of diffuse to global irradiance during the afternoon of the previous day (see Figure 13). This shows the limitation of these cloudy sky correlations.

8. Results from PVT measurements within the home+ building

In June 2010 the twelve large PVT modules on the Home+ building were measured in Madrid/Spain during the Solar Decathlon competition.

Whereas the photovoltaic module temperature was above 70°C during the day and ambient air temperatures at 35°C , the night cooling was very efficient with temperature reduction of the storage tank water from 40°C to 20°C (see Figure 14). During the day the storage tank was used to take up the rejected heat from the compression chiller.

When the PVT collectors were connected to the storage tank, the cooling power was determined from the change of energy content of the storage tank measured with PT100 temperature sensors at three equidistant levels. On average the cooling power of the PVT collectors was between 43.1 ± 2.9 and $65.6 \pm 3.2 \text{ W m}^{-2}$, when the PVT collectors were connected to the heat sink tank and temperature levels in the tank were between 35 and 40°C at the end of the day. Operation times were between 9.2 and 10.8 hours. The electrical COP's as the ratio of cold produced to the pumping energy needed are excellent with values between 17 and 30.

During the night of 21.-22.6., the PVT collectors were directly used to discharge the PCM ceiling and the radiant floor. Supply water temperatures went down as far as 11°C at the end of the night with return temperatures of the radiant floor 2K higher and from the phase change material ceiling 5 K higher (see Figure 15). The flow rates could not be accurately determined during the competition phase and are only estimated at $10.0 \pm 1.0 \text{ kg m}^{-2} \text{ hr}^{-1}$ based on data taken during commissioning. The return temperature levels from the chilled ceiling/floor vary between 21°C at the beginning of the discharge down to about 15°C at the end of the night and are about 10 K lower than for the connection to the storage tank situation.

Table 3 summarizes the results from the measurements in Spain.

9. Parameter studies using the simulation model

To evaluate the performance of the PVT collectors in different climates, simulation studies with the validated PVT and sky models were carried out. Both a hot/dry and a hot/humid climates (Madrid and Shanghai) are considered. The weather data used for the simulation studies are taken from Meteonorm. The mean ambient temperature of Shanghai is higher than Madrid in summer and colder in winter (see Figure 16). The most significant difference in weather between two cities is humidity. The mean absolute humidity in July and August is 19.3 g kg^{-1} and 15 g kg^{-1} in June and September. On the other hand, during the four summer

months in Madrid the mean absolute humidity is only 7 to 7.5 g kg⁻¹. Figure 17 shows global horizontal irradiation of two cities for whole year. The average irradiance level of Madrid is higher than of Shanghai, especially in summer.

As heat transfer by convection can strongly affect radiative cooling, wind velocity is an important factor. The wind velocity data provided by Meeonorm has been used for the simulation. Since the Meeonorm data are taken from meteorological stations with wind velocities measured at 10 m high, the wind speed was corrected to the building height.

Heating and cooling loads as well as thermal comfort conditions were calculated based on a residential building schedule for two persons. Due to the high insulation standard the heating energy demand is negligible. The electricity balance is positive for both climates in both cases due to the high photovoltaic electricity generation, although it is less favourable in Shanghai, since the electricity consumption due to cooling is higher and the PV generation is lower (see Figure 18). The electricity consumption includes the electrical energy needed to drive the compression chiller.

Humidity is the main factor for comfortable level in comparison of all the results. Whereas the temperature comfort range can be maintained with the system technology used, the humidity levels are often too high in the Shanghai climate (see Figure 19). Also, in the humid climate of Shanghai the indirect evaporative cooling is less efficient and direct humidification of supply air is not possible.

Night sky temperatures are higher in Shanghai, as the skies are often overcast. Therefore the radiant cooling system is much less efficient than in Madrid. The PCM ceiling cannot always be regenerated during the night and the heat rejected from the chiller is not dissipated efficiently. Due to high temperatures in the heat sink tank, free cooling cannot be used as much as in Madrid and the chiller COP is lower. The cooling coil of the air handling unit

(AHU) has to be used in Shanghai in order to provide additional cooling and dehumidify the supply air.

The COP of the reversible heat pump is a function of chilled water temperature and temperature of heat rejection. The supply chilled water temperature to the floor cooling system was kept constant at 18°C, therefore the chilled water inlet temperature to the chiller, which is the return temperature from floor cooling system, was always around 20°C. The temperature in the external circuit of the condenser is controlled by the temperature level in the heat sink tank. The COP's of the reversible heat pump in cooling mode are shown as a function of the two temperature levels (see Figure 20).

The seasonal performance factor (SPF) for the chiller are between 4.2 and 4.3 in Madrid and 3.2 for cooling in Shanghai up to 4.2 for heating operation in Shanghai. The lower SPF for summer operation in Shanghai is due to the fact that the high number of operating hours in summer lead to high heat sink tank temperatures (see Table 4).

The total cooling energy produced by the PVT collectors is 52 kWh m⁻² in Madrid and 55 kWh m⁻² in Shanghai. The operating hours are longer in Madrid than in Shanghai, whereas the mean cooling power is higher in Shanghai. This is due to the fact the the PVT cooling is mainly used to regenerate the heat sink tank, which takes up the compression chiller heat during the day and is at a higher temperature level than the PCM ceiling operation. In Madrid convective heat transfer causes night heat gains to the PVT, i.e. it reduces the cooling power. The average convective gains are -13.5 W m⁻². Under Shanghai conditions with higher average PVT night temperatures (re-cooling of heat sink tank), the convective heat transfer to ambient air is positive, i.e. there are heat losses, which increase the cooling power on average by 10 W m⁻² (see Table 5). The average heat sink temperature under summer conditions when the pump is ON is 20.9°C in Madrid and 30.1°C in Shanghai. The specific cooling energy

delivered from the PVT collectors to the PCM ceilings during summer is 16.5 kWh m^{-2} in Madrid and 7.1 kWh m^{-2} in Shanghai, as the nightly fluid temperatures are often not low enough to discharge the PCM ceilings and also the priority was given to cool down the tank when the temperature inside the tank was above 45°C .

A further 35 kWh m^{-2} are supplied to the heat sink tank in Madrid, of which 9.7 kWh m^{-2} can be directly used to cool the 30 m^2 radiant floor. The remaining cooling energy is used for heat rejection of the chiller and includes all other unwanted heat gains.

The PVT driven PCM ceiling covers 27% of the total building cooling energy demand of $39 \text{ kWh m}^{-2} \text{ a}^{-1}$ in the Madrid climate. Free cooling via the radiant floor using water below 19°C temperature from the heat store supplies a further 16% of the building cooling demand. Another 27% of the cooling demand is supplied by a reversible heat pump, and 23 % by indirect evaporative cooling of the ventilation supply air. 6% of the total cooling energy can be provided by direct supply air evaporation. Due to the re-cooling of the heat store by the PVT collectors, the reversible heat pump reaches a very good average seasonal performance factor (SPF) of 4.25 for heating and cooling.

In the warmer Shanghai climate, the direct use of cooling energy within the PCM ceiling is lower and covers only 11% of the total cooling energy demand. Also direct cooling with the radiant floor contributes only 6%. The main contribution to the cooling energy is provided by the reversible heat pump (81%), which has a satisfactory average SPF of 3.2.

10. Conclusions

A new concept for photovoltaic thermal collectors was developed with the goal of providing both electrical and cooling energy for buildings. Radiative heat exchange with the night sky

provides average cooling power of 41 W m^{-2} in central Spanish climate conditions with an average tank temperature of 20.9°C , where the cooling energy can be used for direct cooling of activated floors or ceilings. Under Shanghai climatic conditions the average cooling power is higher at 61 W m^{-2} with an average tank temperature of 30.1°C , as the PVT cooling energy is mainly used to night cool a heat sink storage tank, which takes up heat from an electrical compression chiller. Prototype modules were tested in Stuttgart to validate a simulation model, which showed good agreement between simulated and measurement values. Large PVT modules were then developed and implemented in a zero energy building and tested during Spanish summer conditions. Depending on the temperature level, cooling power levels of 60 to 65 W m^{-2} on average were obtained during one week of measurements. The simulated annual cooling energy for Madrid and Shanghai climatic conditions is between 50 and 55 kWh m^{-2} , which adds to the AC electrical energy of the PVT modules, which is $205 \text{ kWh m}^{-2} \text{ a}^{-1}$ in Madrid and $163 \text{ kWh m}^{-2} \text{ a}^{-1}$ in Shanghai.

Acknowledgements

The work was carried out in the framework of the student competition Solar Decathlon 2010, financially supported by the German Ministry of Economy and Technology.

The work would not have been possible without the very engaged project leadership of our architectural faculty headed by Prof. Dr. Jan Cremers and Sebastian Fiedler. Many thanks to Simon Büttgenbach for his experimental work on the PVT collectors.

References

- [1] Argiriou, A., Santamouris, M., Assimakopoulos, D. N. (1994), Assessment of the radiative cooling potential of a collector using hourly weather data, *Energy*, Volume 19, Issue 8, August 1994, Pages 879-888
- [2] ASHRAE Handbook – Fundamentals, Chapter 3: Heat transfer, 2005.
- [3] Atwater, M.A.; Ball, J.T (1978) Computation of IR sky temperature and comparison with surface temperature. *Solar Energy*, 21, pp.211-216
- [4] Aubinet, M. (1994) Longwave sky radiation parametrizations. *Solar Energy*, 53, 2, pp. 147-154
- [5] Beck, A.; Büttner, D.: Radiative cooling for low energy cold production (2006), Publications of the Hochschule für Technik Stuttgart, Volume 80, Proceedings of the annual building physics symposium
- [6] Berdahl, P., Fromberg R. (1982) The thermal radiance of clear skies. *Solar Energy* 29, pp. 299-314
- [7] Berdahl, P., Martin, M. (1984) Emittance of clear skies. *Solar Energy*, 32, 5, pp.663-664
- [8] Berdahl, P., Martin, M. (1984) Characteristics of infrared sky radiation in the United States. *Solar Energy*, 33, 3/4, pp.321-336
- [9] Berger, X., Buriot D., Garnier, F. (1984) About the equivalent radiative temperature for clear skies. *Solar Energy* 32, pp. 725-733.

- [10] E. Bertram, M. Stegmann, J. Scheuren, C. Rosinski, K. Kundmüller; Unglazed Photovoltaic Thermal collectors in heat pump systems, Proceedings Eurosun 2010, Graz, Austria, 2010.
- [11] Bertram E., Glombin J., Scheuren J., Rockendorf G. “Condensation heat gains on unglazed solar collectors in heat pump systems”, Proceedings of the Eurosun 2010, Graz, Austria 2010.
- [12] Bird RE, Hulstrom RL (1981) A simplified clear sky model for direct and diffuse insolation on horizontal surfaces. Golden, CO: Solar Energy Research Institute; SERI Technical Report SERI/TR:642-761.
- [13] Bliss, R. (1961) Atmospheric radiation near the surface of the ground: a summary for engineers. Solar Energy 5, pp.103.120, 1961.
- [14] Brunt, D. (1932) Notes on radiation in the atmosphere, Quarterly Journal of the Royal Meteorological Society, 58,pp. 389-418
- [15] Brunold, S. (1989) Untersuchungen zum Potential der Strahlungskuehlung in Ariden Klimazonen University of Freiburg, Freiburg, p. Diploma thesis.
- [16] Cavelius, Ralf, Isaksson, Charlotta, Perednis, Eugenijus, Read, Graham E. F. (2005) Passive cooling technologies, Austrian Energy Agency, 125 pages
- [17] Chen, H., Riffat. S.B., Mempoou, B. (2010) Numerical Study on the Energy Performance of a Novel Direct Expansion PV/T Heat Pump (DX-PV/THP) System,

Proceedings of SET2010 - 9th International Conference on Sustainable Energy Technologies;
Shanghai, China.

24-27 August, 2010

[18] Clark, G., Allen C.P. (1978) The estimation of atmospheric radiation for clear and cloudy skies". Proc. 2nd Nat. Passive Solar Conf. 2, 676

[19] Cristofari, C., Notton, G., Canaletti, J.L. (2009) Thermal behavior of a copolymer PV/Th solar system in low flow rate conditions, Solar Energy 83, pp 1123–1138

[20] Dimoudi, Androutsopoulos, A. (2006), The cooling performance of a radiator based roof component, Solar Energy 80 (2006) 1039–1047

[21] Duffie and Beckmann (2006) Solar engineering of thermal processes, Wiley, 3rd Edition

[22] Elsasser, W. M. (1942) Heat transfer by infrared radiation in the atmosphere. Harvard Univ. Met. Studies N°6, Milton, Massachussets

[23] Erell, E., Etzion, Y. (1992) A radiative cooling system using water a heat exchange medium, Architectural Science Review, vol. 35, p.39-49,

[24] Erell, E., Etzion, Y. (2000) Radiative cooling of buildings with flat plate collectors, Building and Environment, Vol. 35, p. 297-305.

[25] Fang, G., Hu, H., Liu, X. (2010) Experimental investigation on the photovoltaic–thermal solar heat pump air-conditioning system on water-heating mode, *Experimental Thermal and Fluid Science* (2010) in press

[26] Farahania, M.F., Heidarinejada, G., Delfanib, S. (2010) A two-stage system of nocturnal radiative and indirect evaporative cooling for conditions in Tehran, *Energy and Buildings* 42 (2010) 2131-2138

[27] Fuentes, M.K. (1987) A simplified thermal model for flat plate photovoltaic arrays, Sandia Report SAND85-0330-UC-63, Albuquerque, N.M.

[28] Hansen J, Sørensen H, Byström J, Collins M, Karlsson B. (2007) Market, modelling, testing and demonstration in the framework of IEA SHC Task 35 on PV/thermal solar systems. In: 22nd European photovoltaic solar energy conference and exhibition, DE2–5, Milan, Italy; September 3–7

[29] Jaikla, S., Nualboonrueng, T., Sichanugrist, P. (2005), Amorphous-Silicon Photovoltaic/Thermal Solar Collector in Thailand, Photovoltaic Specialists Conference, 2005. Conference Record of the Thirty-first IEEE, pp 1687 - 1689

[30] Juchau, B. (1981). Nocturnal and conventional space cooling via radiant floors, *International Passive and Hybrid Cooling Conference*, Miami Beach

[31] Kasten, F., Czeplak, G. (1980) Solar and terrestrial dependent on the amount of the type of cloud, *Solar Energy*, 24, pp. 177-188

[32] Lee, B., Liu, J. Z. , Sun, B., Shen, C. Y., Dai, G. C. (2008) Thermally conductive and electrically insulating EVA composite encapsulants for solar PV cells, eXPRESS Polymer Letters, Vol. 2, N° 5, p.357-363

[33] Meir, M. G., Rekstad, J. B., LØvvik, O.M. (2002) A study of a polymer based radiative cooling system, Solar Energy Vol. 73, No. 6, pp. 403–417, 2002

[34] Perraudau, M. (1986) Climat lumineux à Nantes, resultants de 15 mois de mesures. CSTB EN-ECL 86.14L.

[35] Santamouris, Mat (2007) Advances in passive cooling, Buildings, Chapter 7, Radiative cooling, Energy and Solar Technology Series, ISBN 1844072630

[36] Swinbank, W. (1963) Long-wave radiation from clear skies. Quarterly Journal of Royal Meteorological Society 89, pp. 339-348

[37] Tripanagnostopoulos, Y (2007) Aspects and improvements of hybrid photovoltaic/thermal solar energy systems, Solar Energy 81, pp 1117–1131

Table 1: Main physical parameters of the PVT prototype collector model

PVT module area (m ²)	38
PV cover emissivity (-)	0.85
Absorber emissivity (-)	0.03
Roof emissivity (-)	0.1
Thickness of PV cover (Glazing+cells+glue) (m)	0.016
Thickness of absorber (m)	0.0002
Distance between pipes (m)	0.1
Pipe internal diameter (m)	0.015
Bond conductance of the pipe/absorber contact (W/(mK))	300
Thermal conductivity of the PV cover (Glazing+cells+glue) (W/(mK))	0.79
Thermal conductivity of the absorber (W/(mK))	220

Table 2: clear sky models

Authors	Correlation
Swinbank [36]	$T_{\text{sky}}=0.0552 T_{\text{amb}}$
Fuentes [27]	$T_{\text{sky}}=0.037536 T_{\text{amb}}^{1.5}+0.32 T_{\text{amb}}$
Bliss [13]	$\epsilon_{\text{sky}}=0.8004+0.00396 T_{\text{dp}}$
Elsasser [22]	$\epsilon_{\text{sky}}=0.21+0.22 \ln(p_d)$
Berdahl (night time) [6]	$\epsilon_{\text{sky}}=0.741+0.0062 T_{\text{dp}}$
Berdahl (day time) [6]	$\epsilon_{\text{sky}}=0.727+0.0060 T_{\text{dp}}$
Berdahl (mean) [6]	$\epsilon_{\text{sky}}=0.734+0.0061 T_{\text{dp}}$
Clark and Allen [18]	$\epsilon_{\text{sky}}=0.787+0.0028 T_{\text{dp}}$
Berger et al. [9]	$\epsilon_{\text{sky}}=0.770+0.0038 T_{\text{dp}}$
Brunt [14]	$T_{\text{sky}}=(0.564+0.059 (p_d)^{1/2})^{1/4}$ $T_{\text{sky}}=(0.527+0.065 (p_d)^{1/2})^{1/4}$
Berdahl and Martin [7]	$\epsilon_{\text{sky}}=0.711+0.56 (T_{\text{dp}}/100)+0.73 (T_{\text{dp}}/100)^2$
Chen [17]	$\epsilon_{\text{sky}}=0.736+0.00571 T_{\text{dp}}+0.3318 10^{-5} T_{\text{dp}}^2$
Berdahl and Martin (corrected) [8]	$\epsilon_{\text{sky}}=0.711+0.56 (T_{\text{dp}}/100)+0.73 (T_{\text{dp}}/100)^2+0.013 \cos(15 t)$ $+0.00012 (p_{\text{atm}}-p_0)$

p_d is the water vapour partial pressure in Pa.

T_{dp} is the dew point temperature of ambient air in K.

p_{atm} is the atmospheric pressure of ambient air in Pa.

p_0 is the atmospheric pressure at zero elevation (see level) in Pa (Typically 10^5 Pa)

Table 3: Summary of measurement results from the Solar Decathlon building in Madrid.

Date	Energy dissipated / kWh	Operation time / h	Mean cooling power / W m ²	E _{elec} pump / kWh	COP _{elec}
19-20th June	23.7	9.5	65.6±3.159	0.81	29.3
21-22th June	13.4	9.2	38.5±3.85	0.78	17.2
22-23th June	24.6	10.6	61.1±2.831	0.90	27.3
23-24th June	17.0	10.4	43.0±2.886	0.89	19.2
24-25th June	25.7	10.8	62.4±2.779	0.92	27.9

Table 4: Seasonal performance factors for the reversible heat pump in different climates using a water storage tank as a heat sink.

	Madrid	Shanghai
SPF heating (-)	4.3	4.2
SPF cooling (-)	4.2	3.2

Table 5: Summary of simulation results for the two climates.

	Madrid	Shanghai
Radiative cooling PVT total (kWh/m ² a)	51.7	55.3
Radiative cooling PVT – PCM ceiling (kWh/m ² a)	16.5	7.1
Radiative cooling PVT – Tank (kWh/m ² a)	35.2	50.0
Tank cooling energy used for radiant floor free cooling (kWh/m ² a)	9.7	3.5
Tank cooling energy used for heat rejection chiller (kWh/m ² a)	16.4	33.0
Mean cooling power PVT total (W/m ²)	41.3	61.3
Mean cooling power PVT – PCM ceiling (W/m ²)	30.7	22.5
Mean cooling power PVT – Tank (W/m ²)	42.8	89.3
Mean convective heat losses (+) or gains (-) (W/m ²)	-13.5	+10.1
Operating hours radiative cooling total (h)	1252	902
Operating hours radiative cooling PCM ceiling (h)	537	315
Operating hours radiative cooling Tank (h)	822	560
Mean electrical COP for cooling of PCM ceiling (-)	13.4	6.6
Mean electrical COP for cooling of Tank heat sink (-)	68.5	75.0
Operating hours radiative cooling total (h)	1275	961

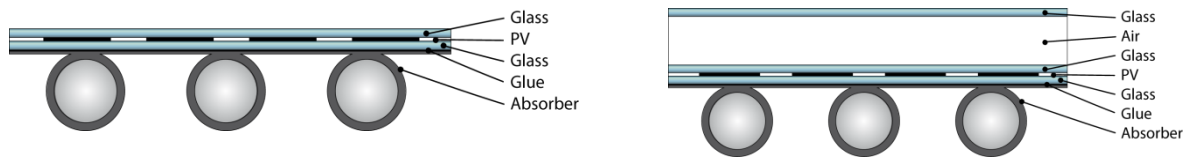


Figure 1: Uncovered and covered PVT collectors



Figure 2: Solar Decathlon Building with PVT roof.

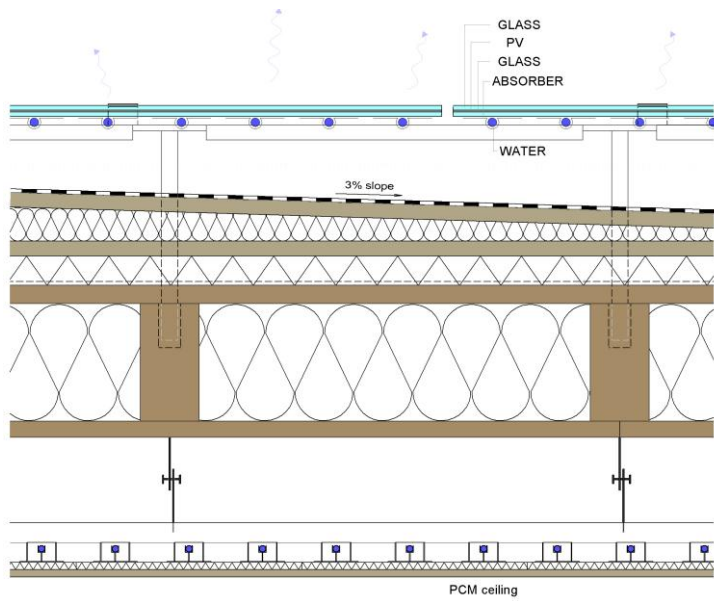


Figure 3: Roof construction of Solar Decathlon Building with PVT collector.

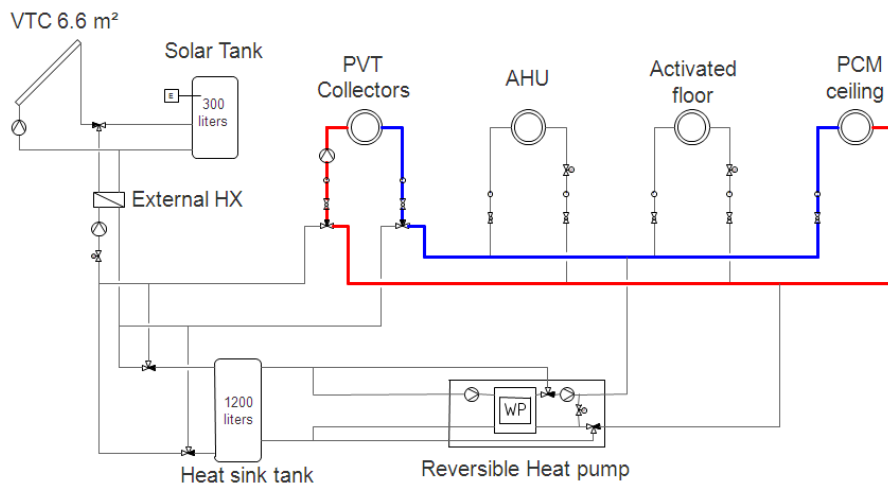


Figure 4: Integration of PVT collectors into the Home+ system technology with vacuum tube collectors and 300 l storage tank for warm water production, PVT collectors, heat sink tank and reversible heat pump, air handling unit AHU, activated floor and PCM ceiling.

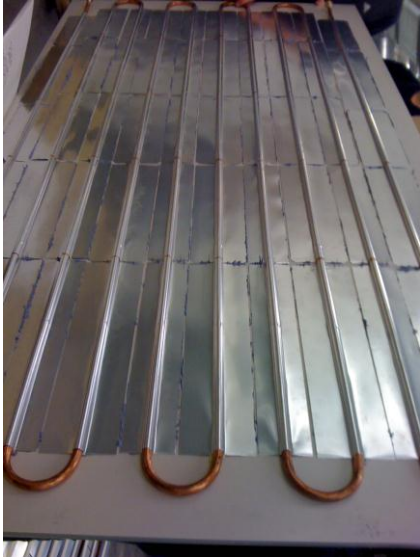


Figure 5: Construction of PVT collector

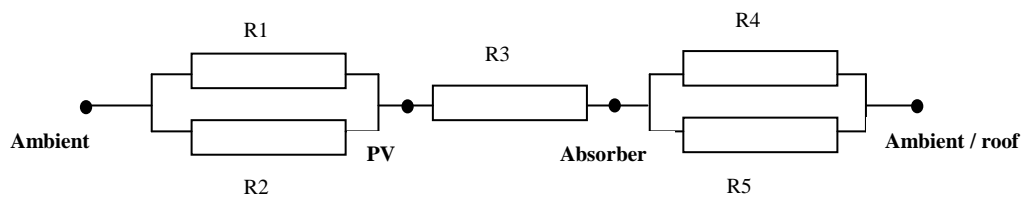


Figure 6: Thermal circuit diagram of the uncovered and non-insulated PVT collector

R1: Thermal resistance of longwave radiation from the PV cover towards the sky

R2: Thermal resistance of mixed convection (free + forced) from the PV cover to the ambient

R3: Thermal resistance of conduction through the PV module + Glue

R4: Thermal resistance of longwave radiation from the absorber towards the roof

R5: Thermal resistance of mixed convection from the absorber to the ambient/roof

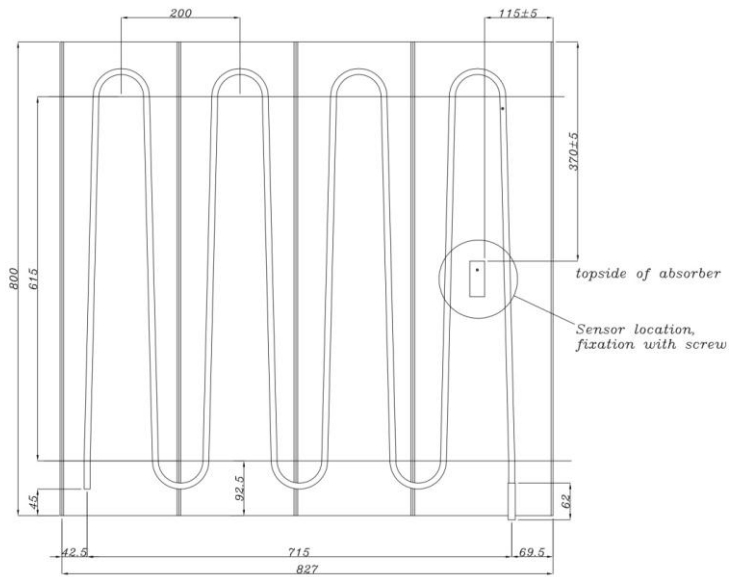


Figure 7: PVT collector dimensions according to the manufacturer (PVTwins)

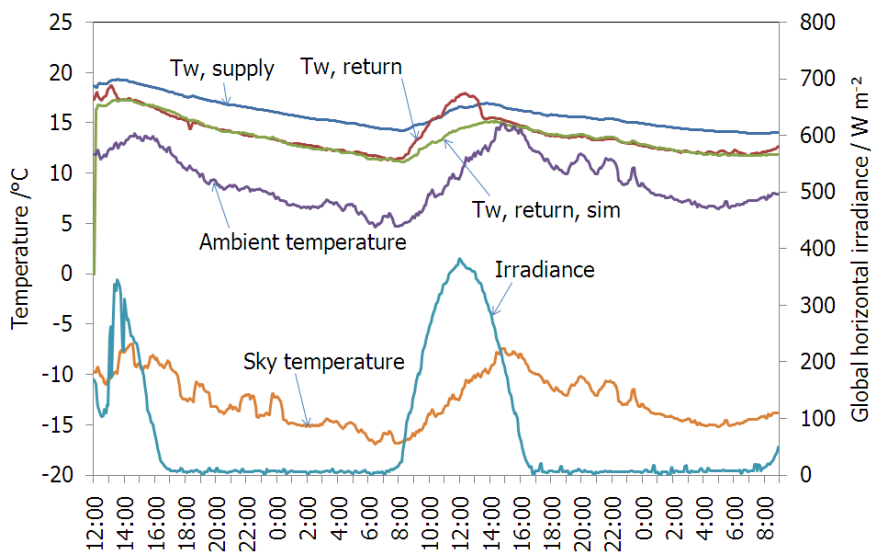


Figure 8: Measured and simulated temperatures of the PVT collector from 18.-20.11.2009 in Stuttgart.

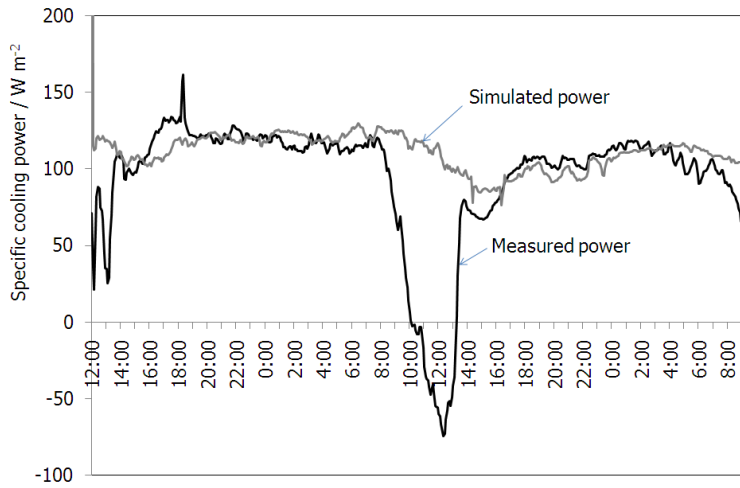


Figure 9: Measured and simulated cooling power for the uncovered PVT collector.

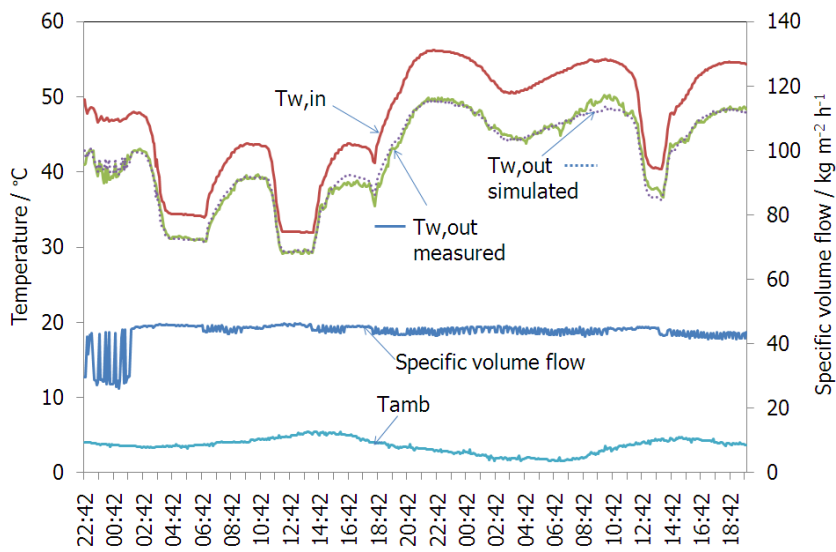


Figure 10: Measured and simulated of PVT collectors at the Stuttgart UAS.

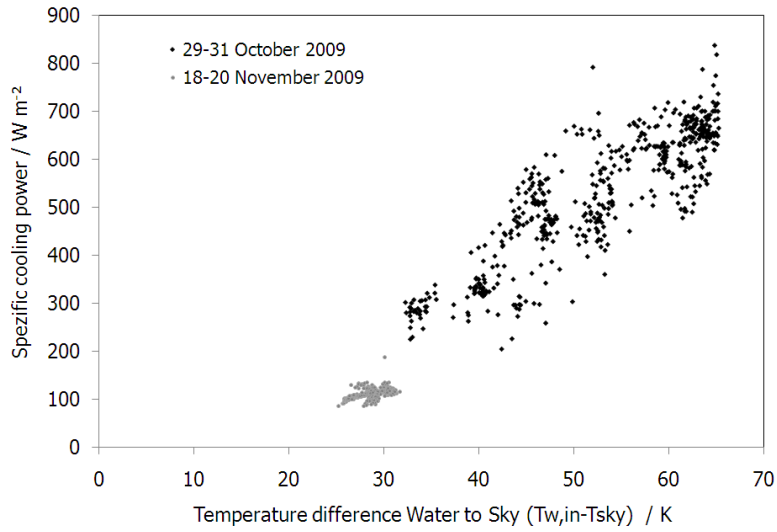


Figure 11: Specific cooling power as a function of measured PVT inlet temperature and sky temperature

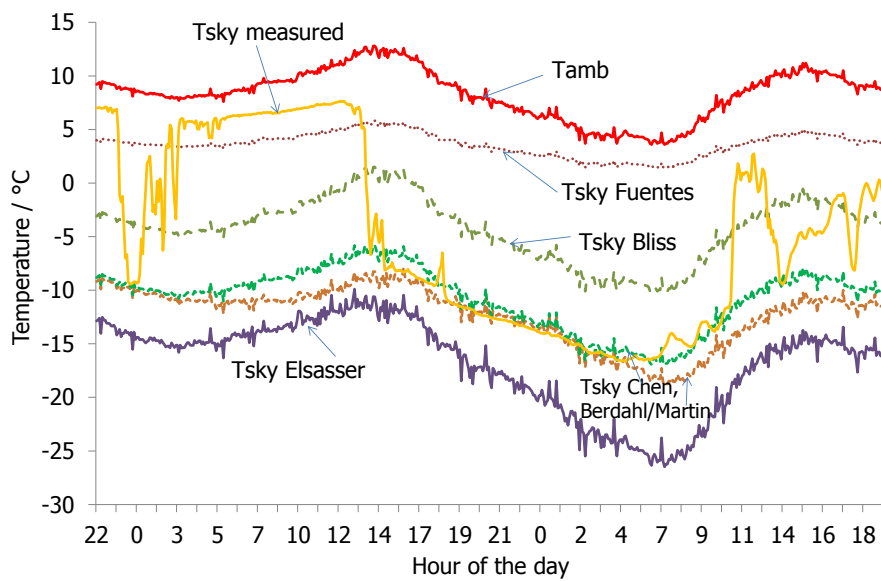


Figure 12: Comparison of measured sky temperature on 29.10.-31.10.2009 with clear sky correlations from the literature.

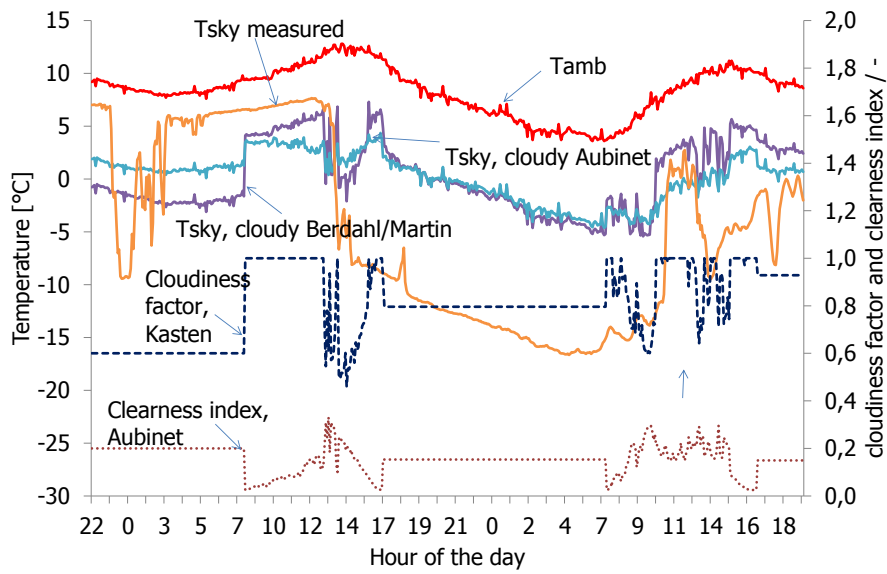


Figure 13: Comparison of measured sky temperature with cloudy sky correlations from the literature.

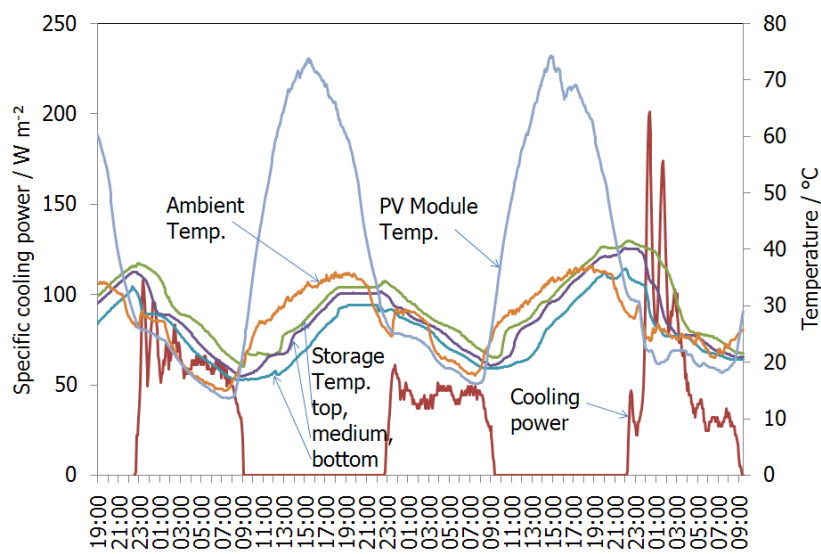


Figure 14: Temperature measurements and obtained cooling power from 22.-25.6.2010 in Madrid when the PVT was connected to the storage tank

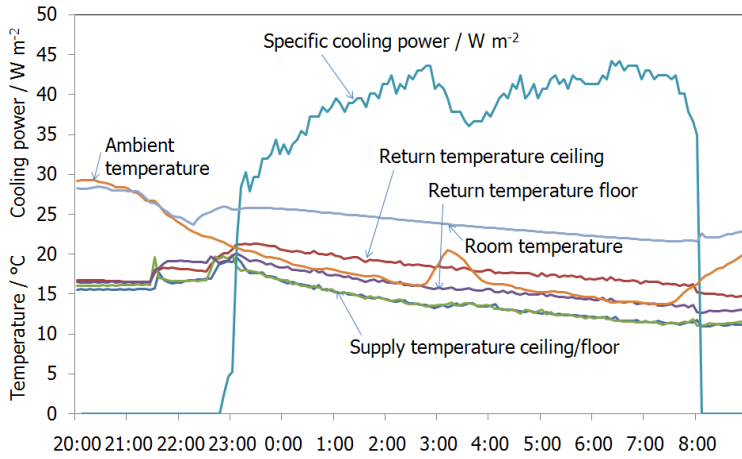


Figure 15: Temperature levels and estimated cooling power when the PVT collectors are directly connected to the radiant floor and PCM ceiling on 21.-22.6.2010.

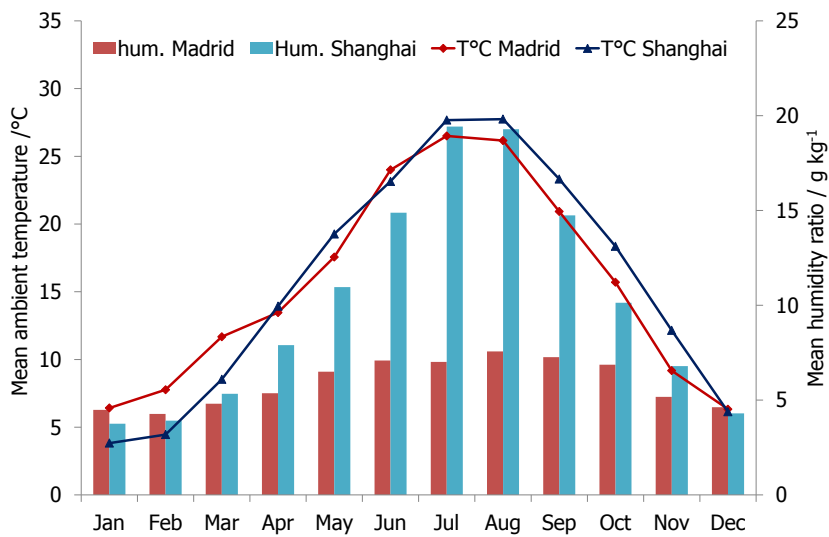


Figure 16: Mean ambient temperature and absolute humidity comparison between Madrid and Shanghai climates.

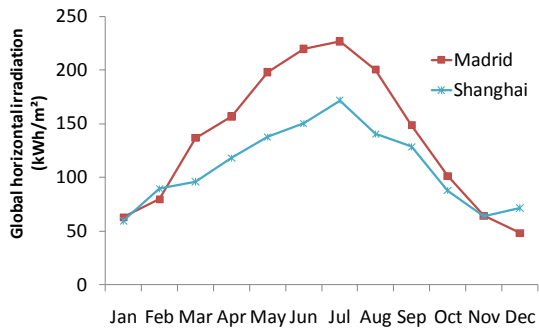


Figure 17: Global horizontal irradiation comparison between Madrid and Shanghai

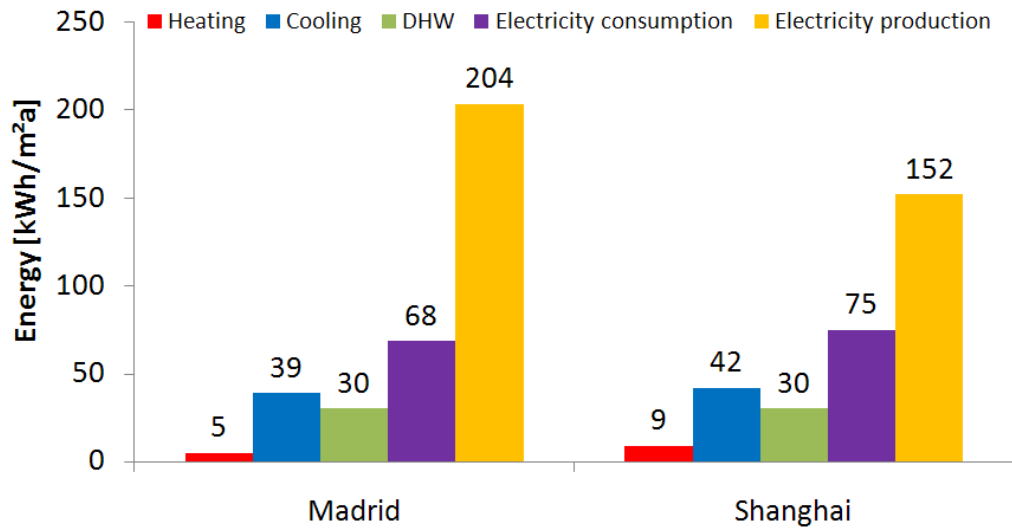


Figure 18: Energy demand and photovoltaic electricity production in both climates.

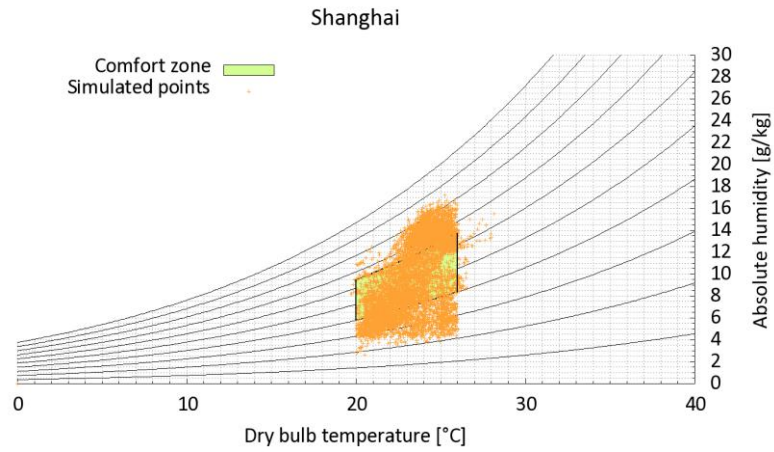


Figure 19: Psychrometric chart and simulated building performance for climatic conditions of Shanghai

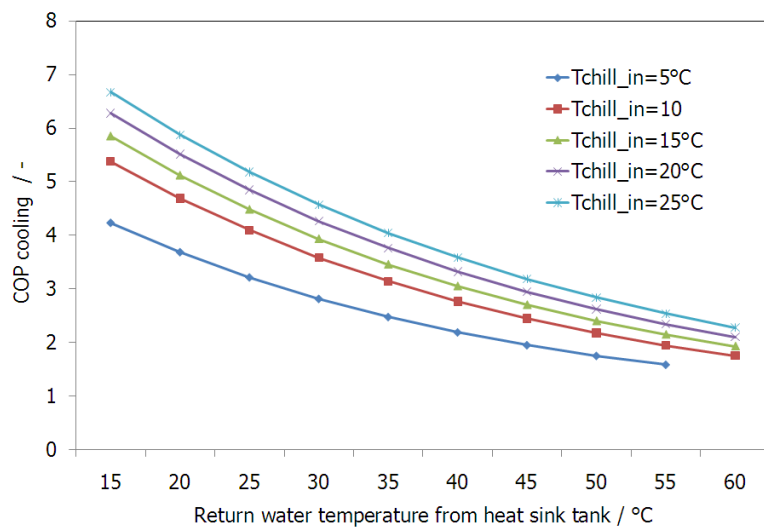


Figure 20: Coefficients of performance of the reversible chiller in cooling mode.